

Coulomb stress interactions among $M \geq 5.9$ earthquakes in the Gorda deformation zone and on the Mendocino Fault Zone, Cascadia subduction zone, and northern San Andreas Fault

John C. Rollins¹ and Ross S. Stein²

Received 8 November 2009; revised 14 June 2010; accepted 8 July 2010; published 3 December 2010.

[1] The Gorda deformation zone, a 50,000 km² area of diffuse shear and rotation offshore northernmost California, has been the site of 20 $M \geq 5.9$ earthquakes on four different fault orientations since 1976, including four $M \geq 7$ shocks. This is the highest rate of large earthquakes in the contiguous United States. We calculate that the source faults of six recent $M \geq 5.9$ earthquakes had experienced ≥ 0.6 bar Coulomb stress increases imparted by earthquakes that struck less than 9 months beforehand. Control tests indicate that ≥ 0.6 bar Coulomb stress interactions between $M \geq 5.9$ earthquakes separated by <9 months are unlikely to occur by random chance, suggesting that the multiple short-term stress interactions observed among the recent Gorda zone earthquakes are not an apparent effect. In all well-constrained ≥ 0.2 bar Coulomb stress interactions between earthquakes that occurred within 4 years of each other, the second earthquake is promoted. On longer timescales, calculated stress changes imparted by the 1980 $M_w = 7.3$ Trinidad earthquake are consistent with the locations of $M \geq 5.9$ earthquakes in the Gorda zone until at least 1995, as well as earthquakes on the Mendocino Fault Zone in 1994 and 2000. Coulomb stress changes imparted by the 1980 earthquake are also consistent with its distinct elbow-shaped aftershock pattern. From these observations, we derive generalized static stress interactions among right-lateral, left-lateral and thrust faults near triple junctions.

Citation: Rollins, J. C., and R. S. Stein (2010), Coulomb stress interactions among $M \geq 5.9$ earthquakes in the Gorda deformation zone and on the Mendocino Fault Zone, Cascadia subduction zone, and northern San Andreas Fault, *J. Geophys. Res.*, 115, B12306, doi:10.1029/2009JB007117.

1. Introduction

[2] The Gorda deformation zone is the southernmost section of the Juan de Fuca plate, bounded by the Gorda Ridge on the west, the Cascadia subduction zone on the east, and the Mendocino Fault Zone on the south (Figure 1). At the southeast corner of the Gorda zone, the North American, Pacific and Juan de Fuca plates meet at the Mendocino Triple Junction. The Juan de Fuca plate generally moves 20°–30° south of east relative to the Pacific plate, but the Mendocino Fault Zone strikes east-west, causing a space problem within the Gorda deformation zone that results in north-south compression and east-west extension. The space problem also slows spreading rates at the Gorda Ridge from 52 mm/yr at 42°N to 25 mm/yr at 40.5°N (Wilson [1989], with Cande and Kent's [1995] timescale correction), which causes the Gorda zone to rotate clockwise. The compression, extension and rotation are accommodated by

internal deformation along northeast striking left-lateral faults [Wilson, 1986; Chaytor *et al.*, 2004]. Since 1976, $M \geq 5.9$ earthquakes have ruptured several of those left-lateral faults as well as the right-lateral Mendocino Fault Zone, the southernmost Cascadia subduction zone, and northwest striking right-lateral faults near Cape Mendocino. In addition, the rupture zone of the 1700 $M \sim 9$ Cascadia earthquake may have extended into this region, and the 1906 San Francisco earthquake ruptured the San Andreas Fault to the Mendocino Triple Junction.

2. Sources for Faults

[3] We use the Chaytor *et al.* [2004] surface traces of the Mendocino Fault Zone and faults in the Gorda deformation zone; those faults are assumed to be vertical. We use the McCrory *et al.* [2004] surface traces of the Gorda Ridge and Cascadia subduction zone. The Cascadia subduction zone dips 9° under northern California [Jachens and Griscom, 1983]; we assume that it strikes 350° in this region (from the surface trace and the Oppenheimer *et al.* [1993] model of the 1992 Cape Mendocino shock) and has a rake of 90°. The northernmost San Andreas and local faults near Cape Mendocino are from the USGS Quaternary Fault and

¹Department of Earth Sciences, University of Southern California, Los Angeles, California, USA.

²U.S. Geological Survey, Menlo Park, California, USA.

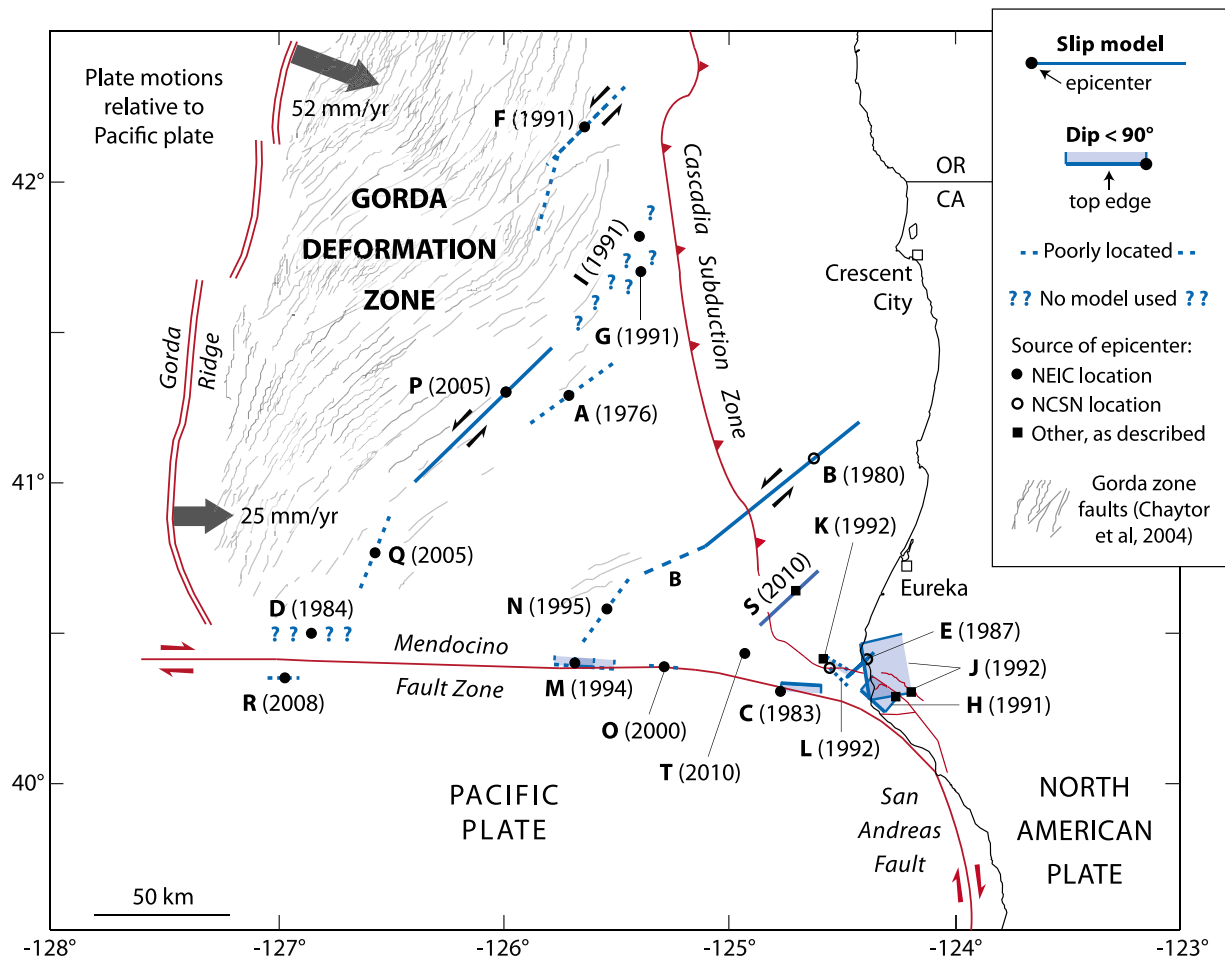


Figure 1. Tectonic configuration of the Gorda deformation zone and locations and source models for 1976–2010 $M \geq 5.9$ earthquakes. Letters designate chronological order of earthquakes (Table 1 and Appendix A). Plate motion vectors relative to the Pacific Plate (gray arrows in main diagram) are from Wilson [1989], with Cande and Kent's [1995] timescale correction.

Fold Database (<http://earthquake.usgs.gov/hazards/qfaults>) and McPherson and Dengler [1992].

3. Source Parameters for 1976–2010 Earthquakes

[4] Because all local seismic stations lie to the east of the offshore Gorda deformation zone, earthquake locations are prone to error, particularly in the east-west direction. We handle these uncertainties on a case-by-case basis for the recent $M \geq 5.9$ earthquakes. The Northern California Seismic Network (NCSN) catalog and the northern California double-difference catalog [Waldhauser and Schaff, 2008] generally provide the most accurate locations for earthquakes close to the coast, but their coverage extends only to 100–150 km offshore; the double-difference catalog is more accurate than NCSN but does not cover the period 1976–1983 (Table 1). The USGS National Earthquake Information Center (NEIC) catalog provides the best locations for earthquakes further offshore, as locations from the underwater SOSUS network appear to have significant westerly biases and magnitude errors in our study area. We obtain aftershock locations for the 1980 $M_w = 7.3$ earthquake from the Hill et al. [1990] plot of 1980–1986 northern California

seismicity (with relocations by J.P. Eaton), as these locations were not incorporated into the NCSN catalog. Unless otherwise indicated, we obtain strike, dip, rake, and scalar moment values for $M \geq 5.9$ earthquakes from the Global CMT catalog. (It should be noted that NCSN and NEIC local magnitudes for two earthquakes in 1983 and 1987 are less than 5.9, but the Global CMT moment magnitudes are 6.1 and 6.0, respectively, so both shocks are included.)

4. Slip Models for 1976–2010 $M \geq 5.9$ Earthquakes

[5] Slip models exist in the literature for the 1992 $M_w = 6.9$ Cape Mendocino, 2005 $M_w = 7.2$, and 2010 $M = 6.5$ earthquakes (Figure 2, Table 1, and Appendix A). For most of the other $M \geq 5.9$ shocks, we construct simple source models using main shock source parameters. For $M < 6.5$ earthquakes, the source length and width are determined by empirical scaling relations from Wells and Coppersmith [1994]. We assume that the seismogenic thickness of the Gorda zone is 9–10 km [Smith et al., 1993; Henstock and Levander, 2003], which constrains the downdip width of $M \geq 6.5$ earthquakes on vertical faults, so for $M \geq 6.5$

Table 1. Source Parameters Used for 1976–2010 $M \geq 5.9$ Earthquakes

ID	Date ^a	General Parameters					Focal Mechanism					Rupture Model Parameters				
		Time (UTC)	M_w	Latitude (°N)	Longitude (°W)	Depth (km)	Reference	Strike	Dip	Rake	Moment (dyn cm)	Reference	Length (km)	Width (km)	Average Slip (m)	Stress Drop (bars)
A	11/26/1976	1119	6.7	41.29	125.71	15	NEIC catalog	54°	85°	5°	1.36×10^{26}	Global CMT NP1	40.0	10.0	1.1	16
B	11/8/1980	1027	7.3	41.085	124.618	14.2	NCSN catalog	51°	89°	27°	1.12×10^{27}	Global CMT NP2	100.0	10.0	3.6	68
C	8/24/1983	1336	6.1	40.31	124.77	30	NEIC catalog	93°	65°	153°	2.09×10^{25}	Global CMT NP1	15.4	7.7	0.6	15
D	9/10/1984	0314	6.6	40.50	126.83	10	NEIC catalog	270°	66°	178°	1×10^{26}	Global CMT NP1	-	-	-	-
E	7/31/1987	2356	6.0	40.416	124.383	17.6	NCSN catalog	226°	90°	0°	1.19×10^{25}	Global CMT NP2	13.2	7.1	0.4	11
F ^b	7/13/1991	0250	6.8	42.182	125.641	11	NEIC catalog	225°	88°	-12°	2.06×10^{26}	Global CMT NP2	40 (1) 55 (2)	10.0 10.0	1.4 (1) 1.1 (2)	27 (1) 20 (2)
G	8/16/1991	2226	6.3	41.697	125.385	10	NEIC catalog	40°	68°	6°	3.13×10^{25}	Global CMT NP1	-	-	-	-
H	8/17/1991	1929	6.1	40.286	124.246	9.3	Walthausser and Schaff [2008]	311°	22°	51°	1.9×10^{25}	Global CMT NP1	12.0	7.7	0.6	22
I	8/17/1991	2217	7.1	41.821	125.397	13	NEIC catalog	46°	86°	28°	4.43×10^{26}	Global CMT NP2	-	-	-	-
J	4/25/1992	1806	6.9	40.301	124.197	9.6	Oppenheimer et al. [1993]	350°	12°	94°	2.79×10^{26}	Oppenheimer et al. [1993]	21.0	16.0	3.3	49
K	4/26/1992	0741	6.5	40.415	124.603	20.4	Walthausser and Schaff [2008]	122.3°	75.9°	175.2°	6.35×10^{25}	Oppenheimer et al. [1993]	12.0	6.4	2.6	78
L	4/26/1992	1118	6.6	40.383	124.555	22.6	NCSN catalog	311.2°	89.6°	181.8°	1.20×10^{26}	Oppenheimer et al. [1993]	10.0	5.0	7.6	290
M	9/1/1994	1515	7.0	40.40	125.68	10	NEIC catalog	274°	65°	176°	3.88×10^{26}	Global CMT NP1	15.0	7.5	10.9	280
N	2/19/1995	0403	6.6	40.56	125.54	10	NEIC catalog	216°	87°	-18°	9.95×10^{25}	Global CMT NP2	30.0	10.0	1.0	19
O	3/16/2000	1519	5.9	40.39	125.28	7	NEIC catalog	275°	88°	180°	7.75×10^{24}	Global CMT NP1	11.3	6.5	0.3	10
P	6/15/2005	0250	7.2	41.29	125.95	16	NEIC catalog	47°	85°	-3°	8.3×10^{26}	Shao and Ji (2005)	72.0	20.0	1.4	21
Q	6/17/2005	0621	6.6	40.77	126.57	12	NEIC catalog	202°	89°	-8°	1.14×10^{26}	Global CMT NP2	30.0	10.0	1.2	23
R	11/28/2008	1342	5.9	40.35	126.98	10	NEIC catalog	270°	85°	176°	1.03×10^{25}	Global CMT NP1	11.8	6.5	0.4	12
S	1/10/2010	0027	6.5	40.652	124.692	29.3	USGS/NEIC	227°	81°	6°	8.0×10^{25}	D. Dreger (unpublished report, 2010)	30.0	20 (max)	0.78	~12
T	2/4/2010	2020	5.9	40.412	124.961	23.6	USGS/NEIC	215°/306°	79°/85°	-5°/-169°	9.19×10^{24}	Global CMT	-	-	-	-

^aDates are given as month/day/year.

^bValues for both models 1 and 2 (as indicated in parentheses) are given for length, average slip, and stress drop.

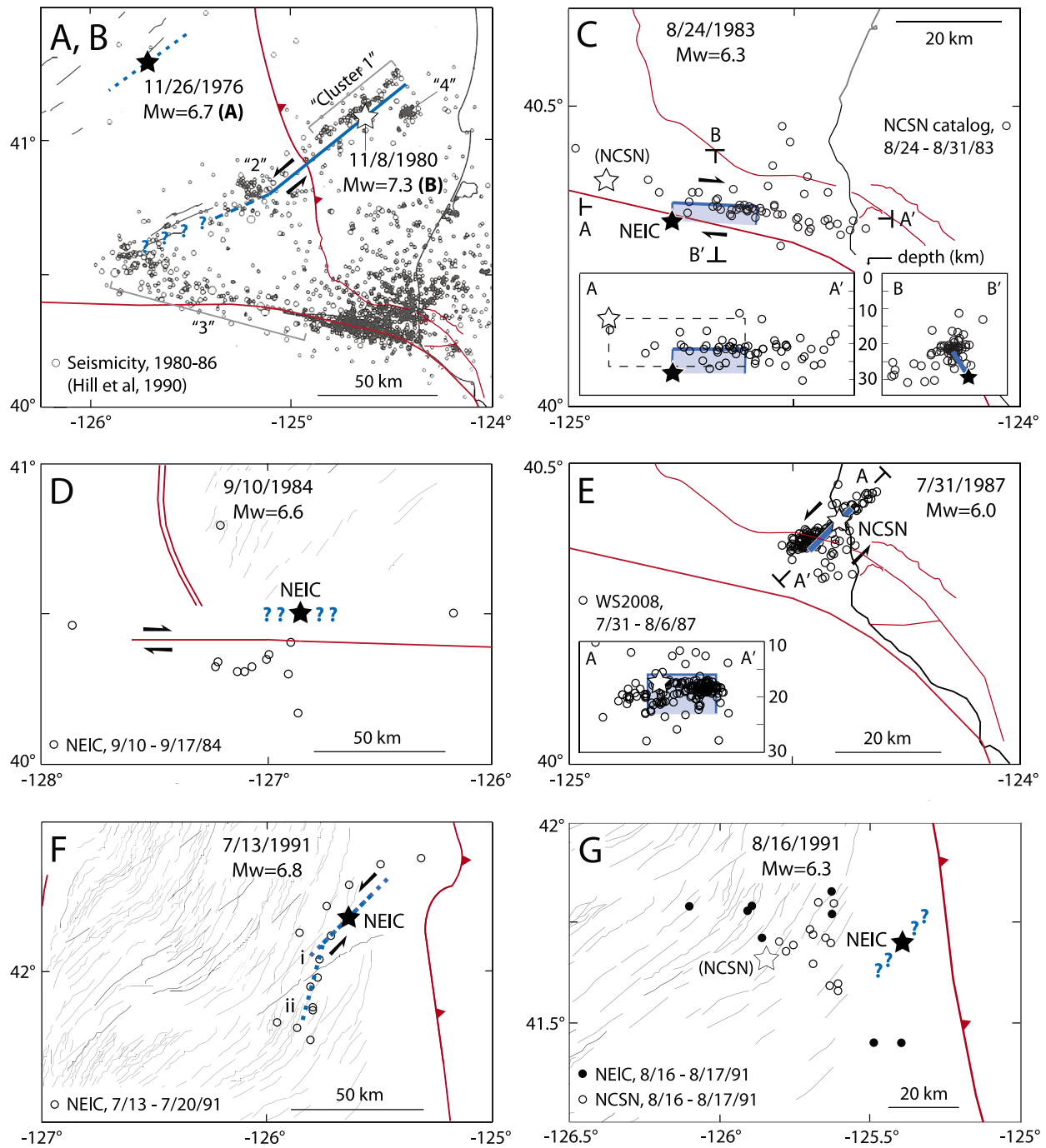


Figure 2. Source models for earthquakes A and B, 26 November 1976, $M_w = 6.7$, and 8 November 1980, $M_w = 7.3$; C, 24 August 1983, $M_w = 6.1$ (poorly constrained); D, 10 September 1984, $M_w = 6.6$ (no model made); E, 31 July 1987, $M_w = 6.0$, “WS2008” refers to *Waldhauser and Schaff’s* [2008] double-difference catalog; F, 13 July 1991, $M_w = 6.8$ (poorly constrained); G, 16 August 1991 (2226 UTC), $M_w = 6.3$ (no model made), open circles are NCSN locations for 16 August 1991 (2226 UTC) to 17 August 1991 (2216 UTC); H, 17 August 1991 (1929 UTC), $M_w = 6.1$; I, 17 August 1991 (2217 UTC), $M_w = 7.1$ (no model made); J, 25 April 1992, $M_w = 6.9$, open circles are from *Waldhauser and Schaff’s* [2008] earthquake locations for 25 April 1992 (1806 UTC) to 26 April 1992 (0741 UTC); K and L, 26 April 1992 (0741 UTC), $M_w = 6.5$ and 26 April 1992 (1118 UTC), $M_w = 6.6$ (both poorly constrained), seismicity shallower than 15 km was excluded so that shallow aftershocks of (J) do not crowd figure; M, 1 September 1994, $M_w = 7.0$; N and O, 19 February 1995, $M_w = 6.6$, and 16 March 2000, $M_w = 5.9$; P, Q, and R, 15 June 2005, $M_w = 7.2$, 17 June 2005, $M_w = 6.6$ (poorly constrained), and 28 November 2008, $M_w = 5.9$ (poorly constrained); S and T, 10 January 2010, $M = 6.5$, and 4 February 2010, $M_w = 5.9$; Z, 18 April 1906, $M = 7.8$.

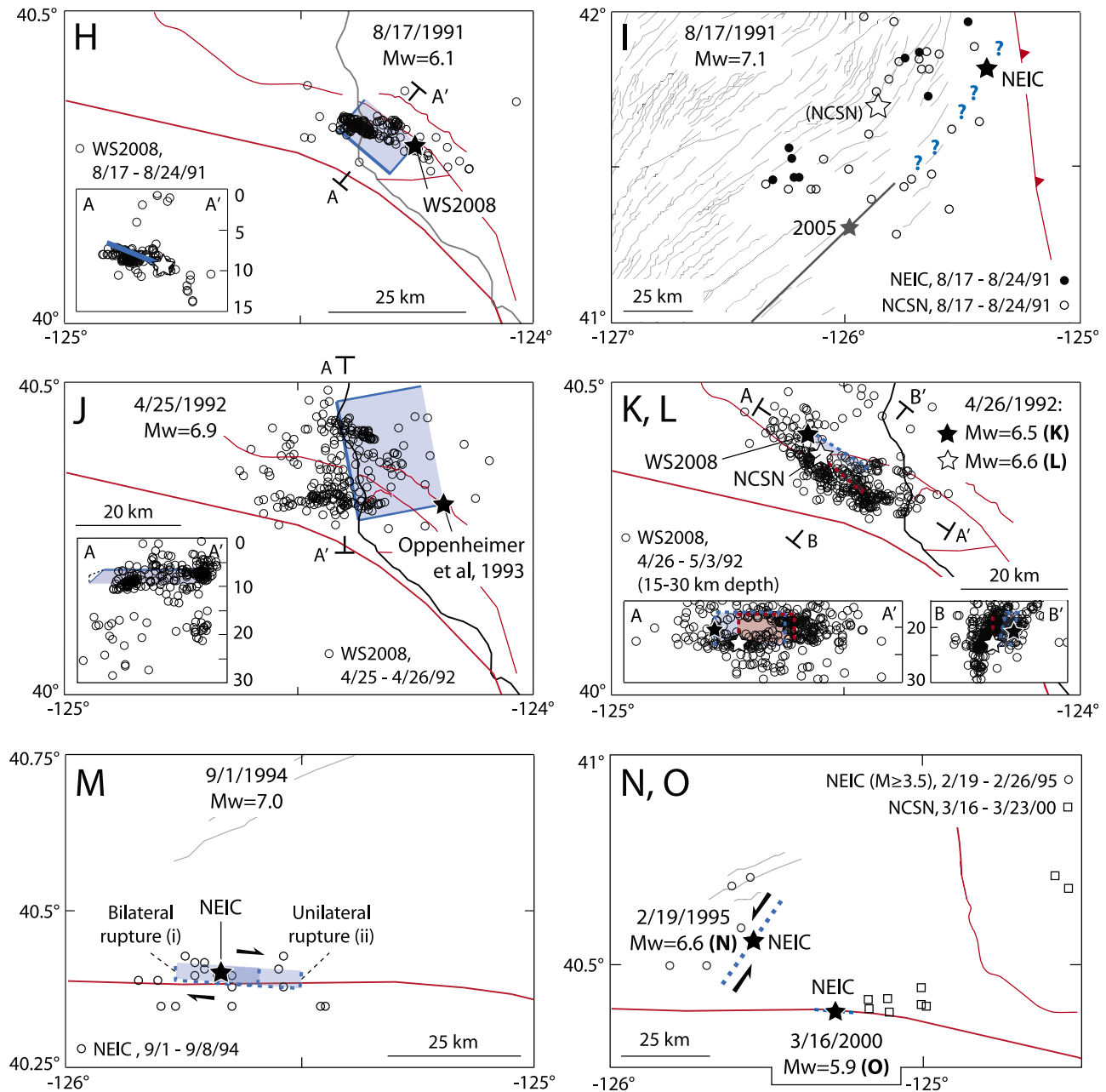


Figure 2. (continued)

earthquakes we assume a width of 10 km and set the source length equal to that of the aftershock pattern. The stress drop is kept between 10 and 100 bars, with the exception of two earthquakes in 1992 and 1994 for which *Choy and McGarr* [2002] observed high apparent stress values. We assume a bilateral rupture if the main shock hypocenter is in the middle of the aftershock pattern and a unilateral rupture if the hypocenter is at one end. If aftershocks are consistent with the best main shock location but do not indicate a fault plane, we conclude that the source model is poorly located, and so stress interactions calculated with it are tentative. If aftershocks are inconsistent with the best main shock location, we do not make a source model for the main shock. All

source models are shown in Figure 2 and described in the Appendix A. The letters used to refer to the earthquakes throughout the rest of the text are keyed to Tables 1 and 2, Figures 1 and 2, and Appendix A.

5. Calculation of Static Stress Transfer

[6] The rupture of a fault in an earthquake deforms the surrounding crust, changing the static stress on nearby faults depending on their orientations. The Coulomb stress change is defined as $\Delta CFF = \Delta\tau + \mu\Delta\sigma$, where τ is the shear stress on the fault (positive in the inferred direction of slip), σ is

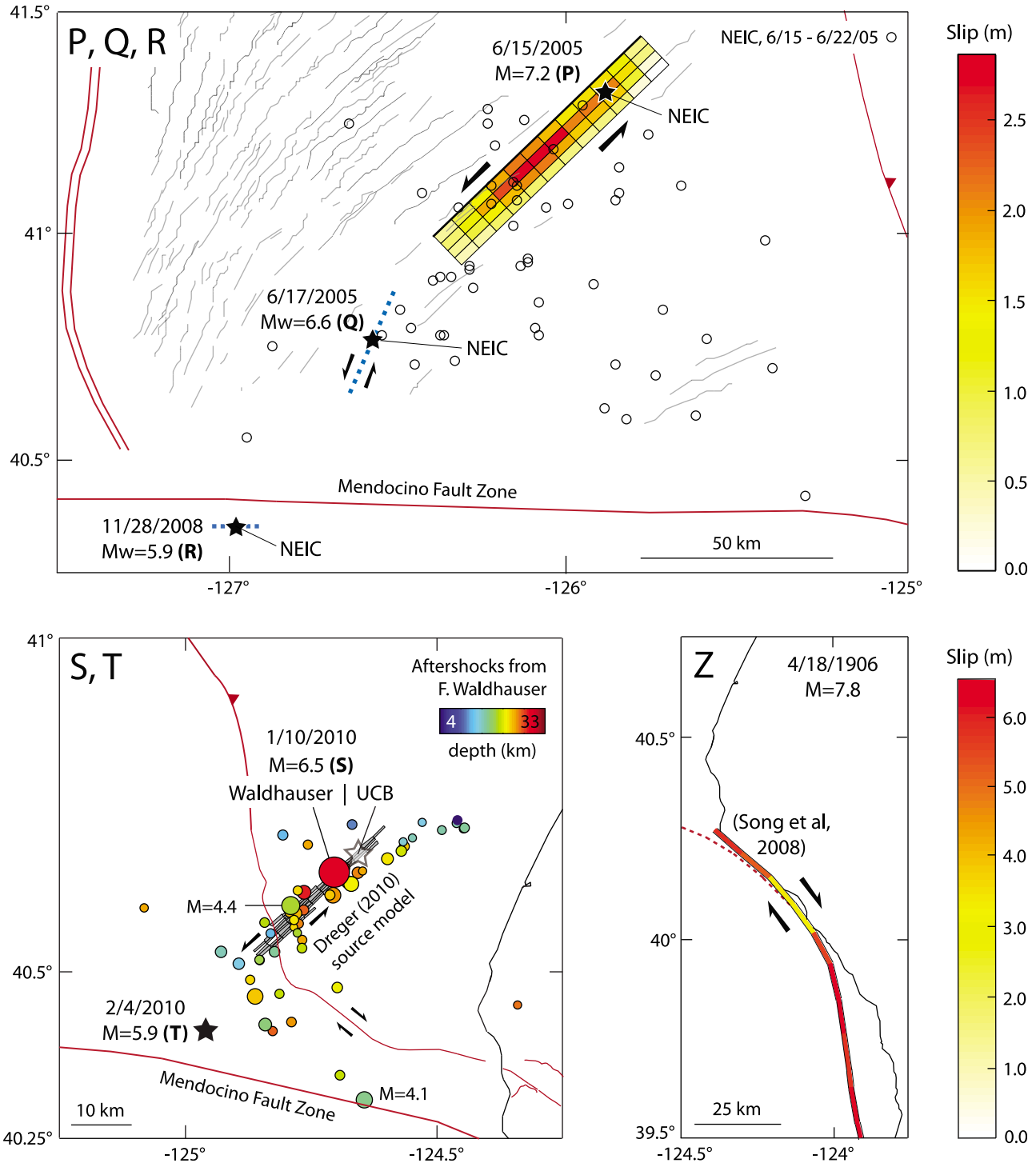


Figure 2. (continued)

the normal stress (positive for unclamping), and μ is the apparent friction coefficient [King *et al.*, 1994].

[7] We perform two kinds of calculations using Coulomb 3.1 (<http://earthquake.usgs.gov/research/modeling/>). The first determines the Coulomb stress change imparted by a source earthquake to the epicenter of a subsequent receiver earthquake given its orientation and rake. The rupture of the

receiver earthquake is promoted if the imparted stress change is positive and inhibited if the stress change is negative. We run this calculation for all source models. The second method determines the stress changes imparted by a source earthquake to surrounding faults; these can be compared with aftershocks and changes in seismicity rates. We run this calculation for the 1980 $M_w = 7.3$, 1992 $M_w = 6.9$,

Table 2. Coulomb Stress Interactions ≥ 0.5 bar Among 1976–2010 $M \geq 5.9$ Earthquakes

Source Earthquake			Receiver Earthquake			Time Between Earthquakes (years)	Imparted Coulomb Stress Change (bars)
ID	Date ^a	M_w	ID	Date ^a	M_w		
A	11/26/1976	6.7	I	8/17/1991	7.1	14.7	Poorly constrained
			P	6/15/2005	7.2	28.5	Likely negative but poorly constrained
B	11/8/1980	7.3	M	9/1/1994	7.0	13.8	+0.7 or more ^b
			N	2/19/1995	6.6	14.3	Large but poorly constrained ^b
			O	3/16/2000	5.9	19.4	+2
			P	6/15/2005	7.2	24.7	-0.5
C	8/24/1983	6.1	K	4/26/1992	6.5	8.7	+0.5 (poorly constrained)
D	9/10/1984	6.6	R	11/28/2008	5.9	24.2	Large but poorly constrained
E	7/31/1987	6.0	L	4/26/1992	6.6	4.7	-2
G	8/16/1991	6.3	I	8/17/1991	7.1	0.003	Large but poorly constrained
H	8/17/1991	6.1	J	4/25/1992	6.9	0.69	+1 (at 1992 epicenter) to +4
I	8/17/1991	7.1	P	6/15/2005	7.2	13.8	Large but poorly constrained
J	4/25/1992	6.9	K	4/26/1992	6.5	0.0016	+0.9
			L	4/26/1992	6.6	0.0019	+3
K	4/26/1992	6.5	L	4/26/1992	6.6	0.0003	Large but poorly constrained
L	4/26/1992	6.6	T	2/4/2010	5.9	17.8	-0.6 on SW striking nodal plane/-0.3 on NW striking nodal plane (poorly constrained)
M	9/1/1994	7.0	N	2/19/1995	6.6	0.47	+3 to +10
			O	3/16/2000	5.9	5.5	+2 to +6
P	6/15/2005	7.2	Q	6/17/2005	6.6	0.006	+1
S	1/10/2010	6.5	T	2/4/2010	5.9	0.06	+0.6 on SW striking nodal plane/+0.9 on NW striking nodal plane

^aDates are given as month/day/year.

^bDepends on rupture length of source and receiver.

and 2010 $M = 6.5$ earthquakes, the only three earthquakes with well-located aftershocks off the likely source fault.

6. Coulomb Stress Interactions Among Recent $M \geq 5.9$ Earthquakes and Faults

[8] We calculate that the following interactions may have occurred among the 20 $M \geq 5.9$ earthquakes since 1976.

[9] 1. The source faults of eight earthquakes (earthquakes J, K, L, M, N, O, Q, and T) may have experienced Coulomb stress increases of ≥ 0.6 bar imparted by previous shocks (Table 3).

[10] 2. In six of those eight cases (J, K, L, N, Q, and T), the source fault ruptured less than 9 months after the imparted stress increase.

[11] 3. In five of the six short-term cases, the imparted Coulomb stress increase was ≥ 0.9 bar. The sixth is the stress change imparted by the January 2010 $M = 6.5$ Ferndale earthquake (S) to the source fault of the February 2010 $M_w = 5.9$ earthquake (T); this stress increase was either 0.6 or 0.9 bar.

[12] 4. The source fault of L (1992) experienced a Coulomb stress decrease of 2 bars imparted by E (1987), the one well-constrained case of an $M \geq 5.9$ earthquake occurring despite a calculated ≥ 0.6 bar stress inhibition (Table 2). However, J (1992) imparted a Coulomb stress increase of 3 bars to the source fault of L.

[13] 5. In all well-constrained ≥ 0.2 bar stress interactions between earthquakes that occurred within 4 years of each other, the second earthquake is promoted. The interaction between Q (2005) and R (2008) is calculated to be a 0.3 bar inhibition but is poorly constrained (Table S4 in the auxiliary material).¹

[14] 6. The epicenters of five $M \geq 5.9$ earthquakes (I, L, N, P, and R) are very close to the inferred rupture areas of previous $M \geq 5.9$ shocks (G, K, B, I, and D, respectively); these five stress interactions were strong but cannot be calculated reliably (Table 2).

Table 3. The Last Imparted ≥ 0.5 bar Stress Changes Before Occurrences of $M \geq 5.9$ Earthquakes

Earthquake			Last ≥ 0.5 bar Coulomb Stress Change (Since 1976) Imparted to Epicenter Prior to Earthquake	
ID	Date ^a	M_w	Earthquake Imparting Stress Change	Magnitude of Stress Change (bars)
A	11/26/1976	6.7	-	-
B	11/8/1980	7.3	-	-
C	8/24/1983	6.1	-	-
D	9/10/1984	6.6	-	-
E	7/31/1987	6.0	-	-
F	7/13/1991	6.8	-	-
G	8/16/1991	6.3	-	-
H	8/17/1991	6.1	-	-
I	8/17/1991	7.1	G (1991)	Large but poorly constrained
J	4/25/1992	6.9	H (1991)	+1 (at epicenter) to +4
K	4/26/1992	6.5	J (1992)	+0.9
L	4/26/1992	6.6	J (1992)	+3
M	9/1/1994	7.0	B (1980)	+0.7
N	2/19/1995	6.6	M (1994)	+3 to +10
O	3/16/2000	5.9	M (1994)	+2 to +6
P	6/15/2005	7.2	I (1991)	Large but poorly constrained
Q	6/17/2005	6.6	P (2005)	+1
R	11/28/2008	5.9	D (1984)	Large but poorly constrained
S	1/10/2010	6.5	-	-
T	2/4/2010	5.9	S (2010)	+0.6/+0.9

^aDates are given as month/day/year.

¹Auxiliary materials are available in the HTML. doi:10.1029/2009JB007117.

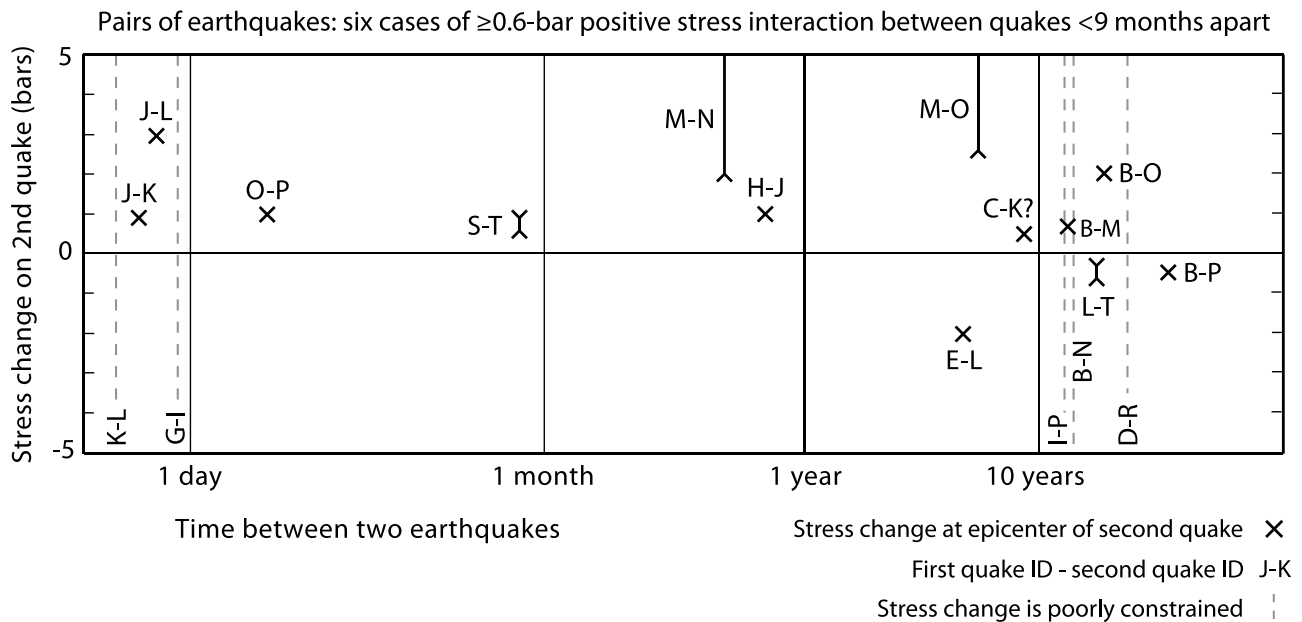


Figure 3. Given any two earthquakes, the first earthquake either promotes the failure of the second by Coulomb stress transfer, inhibits it, or has no effect. Shown here are all pairs of recent $M \geq 5.9$ earthquakes in which the first earthquake is calculated to promote or inhibit the second by ≥ 0.5 bar (Table 2). Each cross represents a pair of two earthquakes. The horizontal axis is the time between the two earthquakes; the vertical axis is the calculated stress change at the epicenter of the second earthquake, given its orientation and rake. Note the six pairs of earthquakes less than 9 months apart in which the first promotes the second by ≥ 0.6 bar.

[15] 7. I (1991) and P (2005) may represent successive ruptures on a single fault, in which case the stress interaction between them would be strong and positive (Figure 1). This may also be true of B (1980) and N (1995).

[16] 8. The other nine $M \geq 5.9$ shocks (A, B, C, D, E, F, G, H, S) did not occur at the sites of ≥ 0.5 bar Coulomb stress interactions imparted by previous earthquakes since 1976 (Table 3), though F may have promoted G by up to 0.3 bar (Table S4).

[17] 9. We calculate that the 1980 $M_w = 7.3$ Trinidad earthquake (B) imparted a Coulomb stress decrease to much of the southern Gorda zone. The locations of $M \geq 5.9$ earthquakes in this area before 1995 (E, F, G, and I) are consistent with the few regions where stress was not decreased in 1980 (Figure 3, Figure 4).

[18] 10. Stress changes imparted by B are also consistent with a band of off-fault aftershocks on and around the Mendocino Fault Zone.

6.1. Stress Changes Imparted by the 9 November 1980, $M_w = 7.3$, Earthquake (B)

6.1.1. Aftershocks

[19] The 1980 Trinidad earthquake (B) produced a distinct elbow-shaped aftershock pattern that included both a main NE trending band of aftershocks on the rupture and a separate WNW trending cluster to the south [Eaton, 1987; Hill *et al.*, 1990] (also relocations by J.P. Eaton using phase data from TERA Corporation and NCSN) (Figure 4). The aftershock clusters are hereafter referred to by the numbering system used in Figures 2 (earthquake A) and 4. The off-fault cluster south of the rupture, labeled “3” in Figures 2 and 4, trends 285° and initially follows the right-lateral

Mendocino Fault Zone but becomes misaligned west of 125.5°W longitude as the fault zone curves due west; the aftershocks taper off at 126°W , 20 km north of the fault zone. The seismicity between 125.5°W and 126°W is either on the Mendocino Fault Zone (with errors in location) or on left-lateral faults just to the north. Our source model for the 1980 main shock increases Coulomb stress on both the Mendocino Fault Zone between 125°W and 125.8°W and nearby left-lateral faults between 125.5°W and 126°W . Thus, seismicity between 125.8°W and 126°W is inconsistent with calculated stress changes if it is on the Mendocino Fault Zone, but the rest of cluster 3 ($>70\%$ of it) is consistent with stress changes regardless of what fault system it occurred on. If seismicity between 125.8°W and 126°W is on left-lateral faults, the entire cluster is consistent with calculated stress changes.

[20] These findings assume that the 1980 rupture did not extend to the Mendocino Fault Zone and is defined only by clusters 1 and 2 to the northeast. If the rupture extended southwest to cluster 3, Coulomb stress would have been increased on the Mendocino Fault Zone between 125°W and 126°W , consistent with some of cluster 3, though aftershocks between 125.5°W and 126°W could be on the rupture. The calculated stress increase between 125°W and 125.8°W on the Mendocino Fault Zone is robust.

[21] In addition to aftershocks on the rupture and the Mendocino Fault Zone, Eaton [1987] and Hill *et al.* [1990] show a localized cluster at ≤ 10 km depth 25 km east of the main $N50^\circ\text{E}$ trend (“4” in Figures 2, earthquake A, and 4). This cluster may be on a separate area of slip in the 1980 main shock, a left-lateral fault parallel to the rupture, the Cascadia subduction zone (the megathrust interface would

Source earthquake: November 8, 1980, $M_w=7.3$ (B)
 Receivers: Mendocino Fault Zone, Cascadia subduction zone, and left-lateral faults

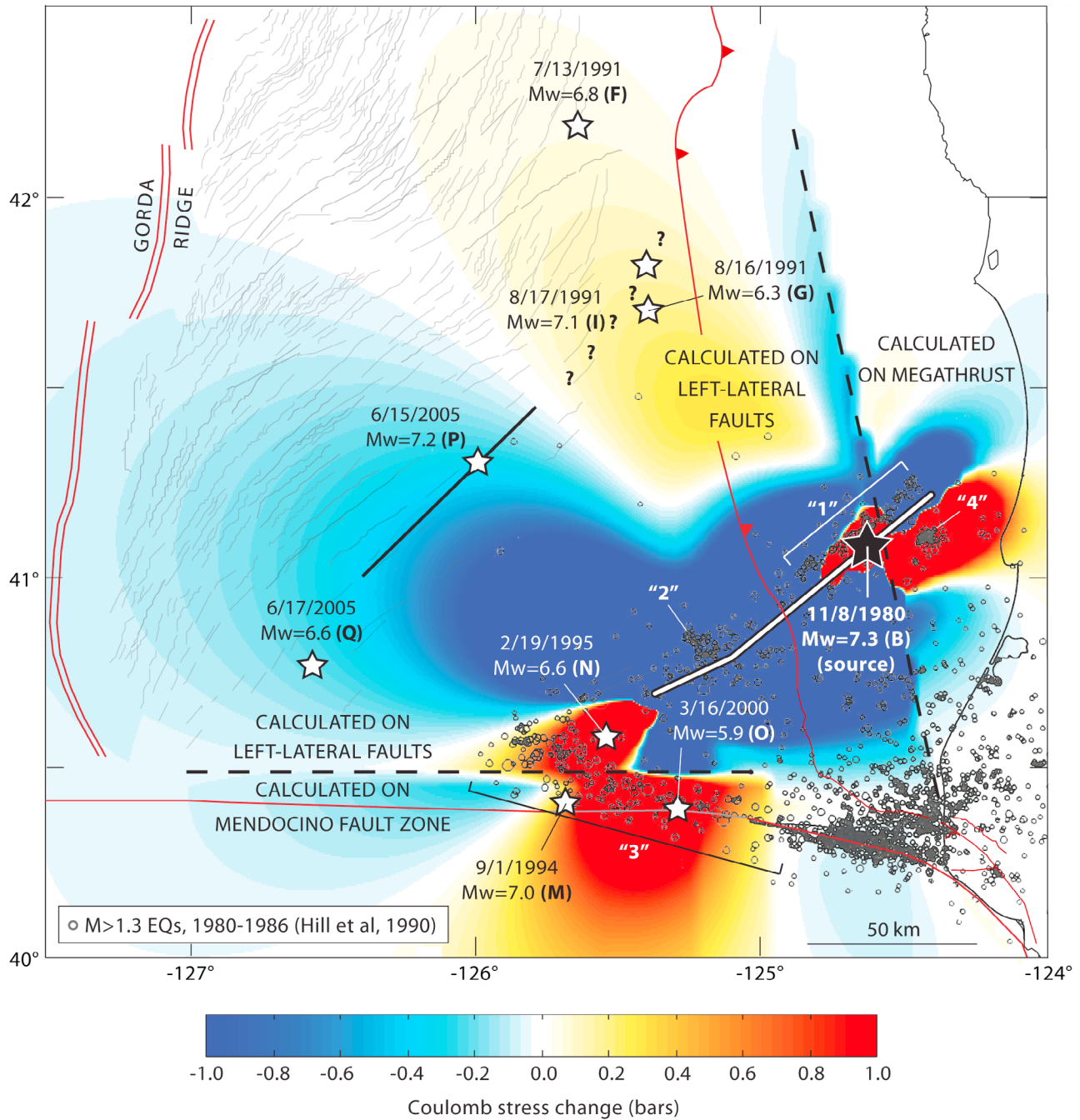


Figure 4. Coulomb stress changes imparted by the 1980 $M_w = 7.3$ earthquake (B) to a matrix of faults representing the Mendocino Fault Zone, the Cascadia subduction zone, and NE striking left-lateral faults in the Gorda zone. The Mendocino Fault Zone is represented by right-lateral faults whose strike rotates from 285° in the east to 270° in the west; Cascadia is represented by reverse faults striking 350° and dipping 9° ; faults in the Gorda zone are represented by vertical left-lateral faults striking 45° . The boundary between the left-lateral “zone” and the reverse “zone” in the fault matrix is placed at the 6 km depth contour on Cascadia, approximated by extending the top edge of the *Oppenheimer et al.* [1993] model for the 1992 Cape Mendocino earthquake (J). Calculation depth is 5 km. The numbered brackets are groups of aftershocks from *Hill et al.* [1990].

be at 7–8 km depth at the location of the cluster), or faults within the overriding North American plate (R. C. McPherson, personal communication, 2010). Our model for the 1980 earthquake increases Coulomb stress on the Cascadia subduction zone in the area of cluster 4 and decreases stress elsewhere on the megathrust, so if cluster 4 is on the megathrust, it is consistent with stress changes imparted by the 1980 earthquake.

6.1.2. Subsequent $M \geq 5.9$ Earthquakes

[22] Two $M \geq 5.9$ earthquakes ruptured the Mendocino Fault Zone between 125°W and 125.8°W after 1980: a $M_w = 7.0$ earthquake at 125.7°W in 1994 (M) and a $M_w = 5.9$ earthquake at 125.3°W in 2000 (O). Our source model for B imparts Coulomb stress increases of 0.7 and 2.0 bars to the epicenters of M and O, respectively (Figure 4).

[23] In 1995, an $M_w = 6.6$ left-lateral earthquake (N) struck near the southwest end of the inferred rupture area of B. Because of uncertainties in locations and rupture areas, the stress interaction between these two earthquakes is not well constrained. However, the location of N suggests that these earthquakes may represent successive ruptures on one fault, in which case the stress interaction between them would have been strong and positive, as in the case of 20th century earthquakes on the North Anatolian Fault [Stein *et al.*, 1997].

[24] Excluding faults to the southwest, we calculate that B decreased Coulomb stress on most left-lateral faults in the southern Gorda deformation zone, producing a “stress shadow.” Four $M \geq 5.9$ left-lateral earthquakes occurred in the Gorda zone between 1980 and 1994: a $M_w = 6.0$ earthquake at Cape Mendocino in 1987 (E) and three $M \geq 6.3$ earthquakes to the north of the 1980 rupture in the summer of 1991 (F, G, and I). We calculate that these shocks all occurred outside of the stress shadow of B: the source fault of E experienced no stress change in 1980, and left-lateral faults in the region in which F, G and I occurred experienced a ≤ 0.2 bar stress increase in 1980. The locations of $M \geq 5.9$ left-lateral earthquakes until at least 1995 were thus consistent with calculated stress changes imparted by B, and if N (1995) occurred on the same fault as B, that stress interaction was positive as well. The first $M \geq 5.9$ earthquake to definitely occur within the calculated 1980 stress shadow was the 2005 $M_w = 7.2$ shock (P).

6.2. Stress Changes Imparted by Earthquake C (1983) to K and L (1992)

[25] The 24 August 1983 $M_w = 6.1$ earthquake (C) occurred near the future site of the 25 April 1992 $M_w = 6.9$ Cape Mendocino earthquake (J) and its two deep $M_w = 6.5$ (K) and $M_w = 6.6$ (L) aftershocks. Our model for C imparts a negligible Coulomb stress change to the source fault of J but increases stress by 0.5 bar at the epicenter of K and decreases stress by 0.4 bar at the epicenter of L (Figure 5c). The interactions with K and L are dependent on the rupture length of C, so they are poorly constrained.

6.3. Stress Changes Imparted by E (1987) to K and L (1992)

[26] Our model for the 31 July 1987 $M_w = 6.0$ Cape Mendocino earthquake (E) decreases Coulomb stress by 0.2 and 2 bars at the epicenters of K and L (1992), respectively (Figure 5c).

6.4. Stress Changes Imparted by the 1991 Honeydew Earthquake (H) to the 1992 $M_w = 6.9$ Cape Mendocino Shock (1992)

[27] Our model for the 17 August 1991 $M_w = 6.1$ Honeydew earthquake (H) increases Coulomb stress by ≥ 1 bar on the southern part of the *Oppenheimer et al.* [1993] rupture surface for the 25 April 1992 $M_w = 6.9$ Cape Mendocino earthquake (J), including a stress increase of 1 bar at the 1992 epicenter.

6.5. Stress Changes Imparted by I (1991) to P (2005)

[28] The location error for the 17 August 1991 $M_w = 7.1$ earthquake (I) is too great for its stress interaction with the 15 June 2005 $M_w = 7.2$ earthquake (P) to be calculated reliably. When compared to *Chaytor et al.* [2004] mapped faults, the NEIC locations for these two earthquakes suggest that they may represent successive ruptures on a single fault (Figure 1), in which case the stress interaction between them would have been strong and positive. If they occurred on parallel but separate faults, the stress interaction could have been either positive or negative depending on their rupture lengths. Earthquakes A (1976) and B (1980) imparted Coulomb stress decreases to the source fault of P; these may have affected the timing of P and may be linked to the 14 year intervening period between I and P.

6.6. Stress Changes Imparted by the 25 April 1992, $M_w = 6.9$, Cape Mendocino Earthquake (J)

6.6.1. Faults Parallel to Source

[29] Small aftershocks of this earthquake are mainly concentrated in two WNW trending linear clusters (Figure 5). If these are taken to represent the northern and southern edges of the rupture plane, the *Oppenheimer et al.* [1993] model is aligned with the southern cluster but somewhat misaligned with the northern cluster. Similarly, Coulomb stress changes imparted to thrust faults are consistent with the southern aftershock cluster but only partially consistent with the northern cluster (Figure 5a).

6.6.2. Stress Changes Imparted to K and L (26 April 1992, $M_w = 6.5$ and 6.6)

[30] The $M_w = 6.9$ Cape Mendocino earthquake (J) was followed 12 and 15 h later by $M_w = 6.5$ (K) and $M_w = 6.6$ (L) aftershocks at 15–25 km depth. Our source model for the $M_w = 6.9$ shock increases Coulomb stress by 0.9 bar at the epicenter of K and by 3 bars at the epicenter of L (Figure 5b). The stress changes imparted to the epicenters of the two aftershocks by earthquakes in 1983 (C) and 1987 (E) may explain why K occurred first even though L was more strongly promoted by J (Figure 5c).

6.7. Stress Changes Imparted by the 1994, $M_w = 7.0$, Mendocino Fault Zone Earthquake (M) to N (1995) and O (2000)

[31] To account for uncertainties in the location of the 1994 $M_w = 7.0$ Mendocino Fault Zone earthquake (M), we made one source model with the NEIC epicenter at the centroid (model 1) and one with the epicenter at the west end (model 2). Model 1 increases Coulomb stress by 3–6 bars at the epicenter of the 1995 $M_w = 6.6$ southern Gorda zone shock (N), and increases stress by 2–3 bars at the epicenter of the 2000 $M_w = 5.9$ earthquake on the Mendocino Fault Zone (O) (Figure 6). Model 2 for the 1994 earthquake

Source: April 25, 1992, $M_w=6.9$, Cape Mendocino, CA (J)

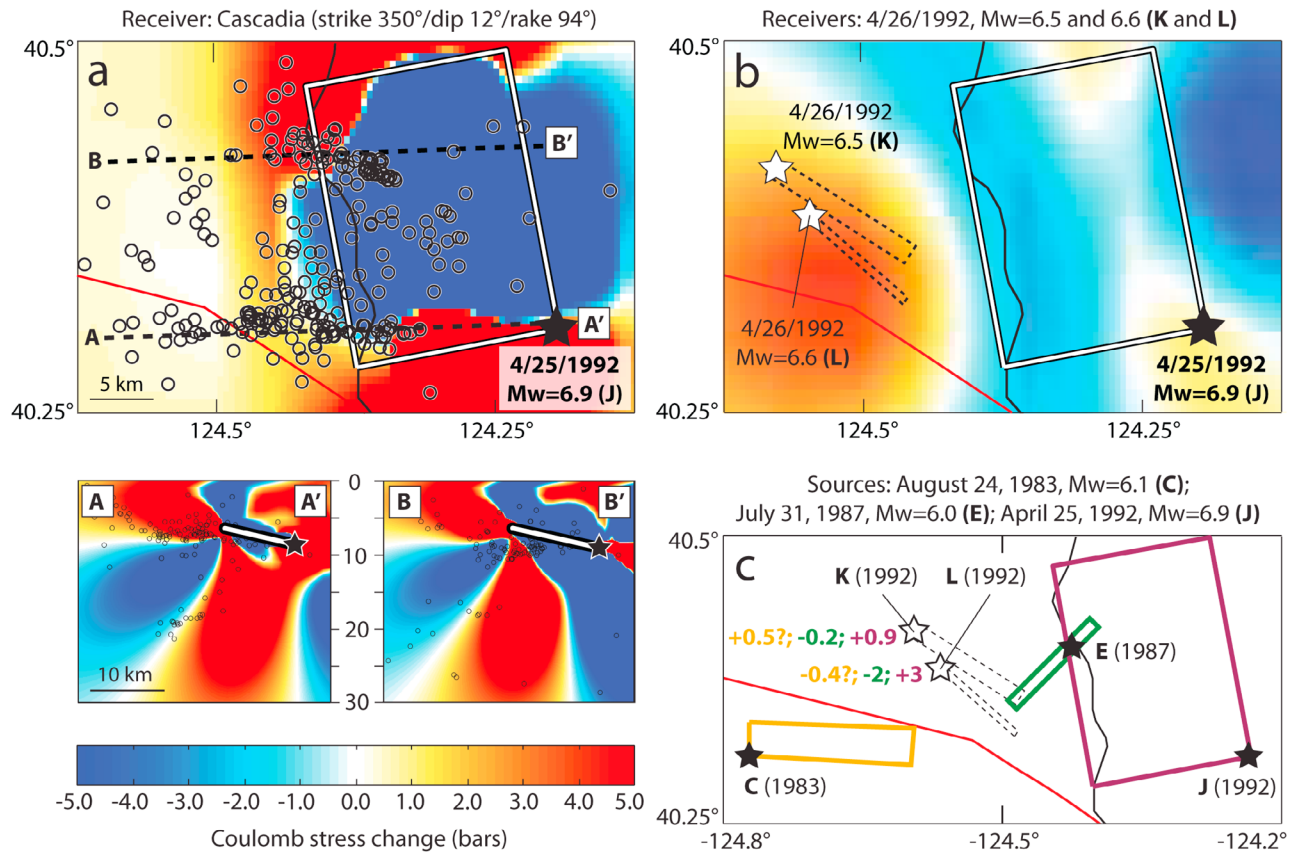


Figure 5. (a) Coulomb stress changes imparted by the 1992 $M_w = 6.9$ Cape Mendocino earthquake (J) to the Cascadia subduction zone. Calculation depth is 8 km. Open circles are *Waldhauser and Schaff* [2008] earthquake locations for 25 April 1992 to 2 May 1992, 0–15 km depth. Seismicity data were cut off at 15 km depth to prevent interference from aftershocks of K and L. Cross section A-A' includes seismicity between 40.24°N and 40.36°N. Cross section B-B' includes seismicity between 40.36°N and 40.48°N. (b) Coulomb stress changes imparted by the 1992 $M_w = 6.9$ earthquake (J) to $M_w = 6.5$ and $M_w = 6.6$ shocks the next day (K and L). Stress change is resolved on the average of the orientations of K and L (strike 127°/dip 90°/rake 180°). Calculation depth is 21.5 km. (c) Calculated Coulomb stress changes imparted by $M \geq 5.9$ shocks in 1983, 1987, and 1992 (C, E, and J) to the epicenters of K and L. The series of three colored numbers represent stress changes imparted by C, E, and J, respectively.

increases stress by 4–10 bars at the epicenter of N and increases stress by 6 bars at the epicenter of O. The stress interaction between earthquakes B (1980) and N is strong but poorly constrained, so the combined stress change imparted to the source fault of N by B and M is unknown. As M occurred much closer in time to N, its stress effect may have been more important than that of B. More robust is the observation that both B and M imparted >1 bar stress increases to the epicenter of O; this is our best constrained interaction on a >10 year timescale.

6.8. Stress Changes Imparted by P (15 June 2005, $M_w = 7.2$) to Q (17 June 2005, $M_w = 6.6$)

[32] The G. Shao and C. Ji (Preliminary result for rupture process of June 15, 2005 $M_w = 7.2$ northern California earthquake, 2005, available at http://www.geol.ucsb.edu/faculty/ji/big_earthquakes/2005/06/smooth/northernca.html, hereafter cited as Shao and Ji, 2005) source model for the

15 June 2005 $M_w = 7.2$ earthquake (P) imparts a Coulomb stress increase of 1 bar to the epicenter of a $M_w = 6.6$ shock to the southwest which occurred 51 h later (Q) (Figure 7). These earthquakes may represent successive ruptures on a single fault; the orientations of local *Chaytor et al.* [2004] faults indicate that the NEIC epicenter for Q would have to be incorrect by ~10 km for the two earthquakes to be on the same fault.

6.9. Stress Changes Imparted by the 10 January 2010, $M = 6.5$ Earthquake (S)

6.9.1. Aftershocks and Cascadia Subduction Zone

[33] The 10 January 2010, $M = 6.5$, earthquake had an L-shaped aftershock pattern, with a main N50°–55°E on-fault trend and a separate N45°W trend at the southwest end of the rupture (Figure 8). We calculate that the main shock increased Coulomb stress on NW striking faults to the southwest, somewhat consistent with the NW trending off-

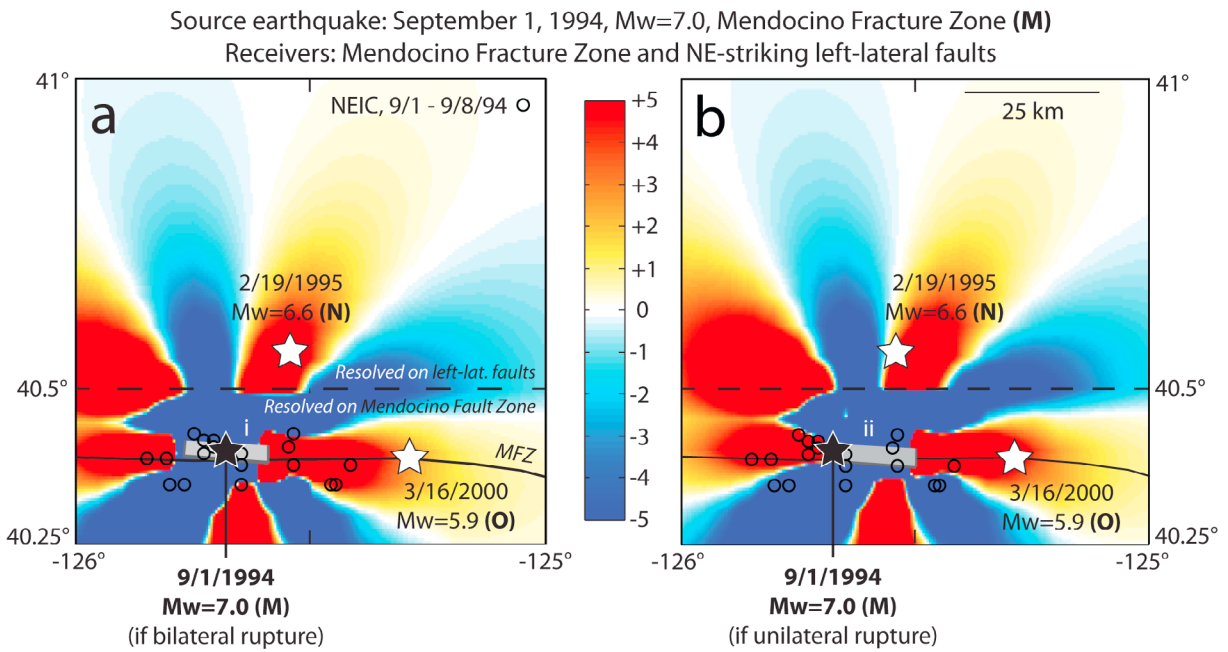


Figure 6. Coulomb stress changes imparted by our models of (a) a bilateral rupture and (b) a unilateral eastward rupture for the 1994 $M_w = 7.0$ Mendocino Fault Zone earthquake to the epicenters of the 1995 $M_w = 6.6$ southern Gorda zone earthquake (N) and the 2000 $M_w = 5.9$ Mendocino Fault Zone earthquake (O). Calculation depth is 5 km.

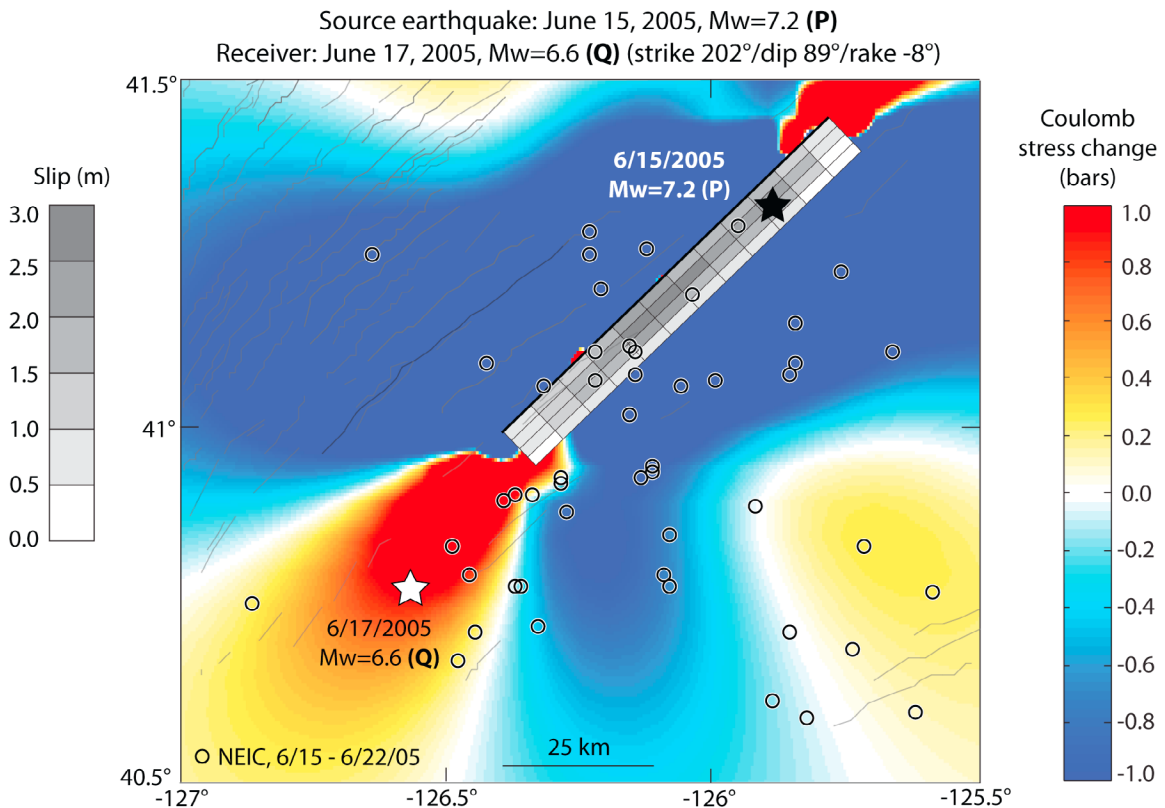


Figure 7. Coulomb stress changes imparted by the Shao and Ji (2005) variable slip model for the 15 June 2005 $M_w = 7.2$ earthquake (P) to the epicenter of the 17 June 2005 $M_w = 6.6$ earthquake (Q). Calculation depth is 10 km.

Source earthquake: January 10, 2010, $M=6.5$ (S)
 Receivers: February 4, 2010 $M_w=5.9$ quake (T), nodal plane 2 (strike 306°/dip 85°/rake -169°),
 and Cascadia subduction zone

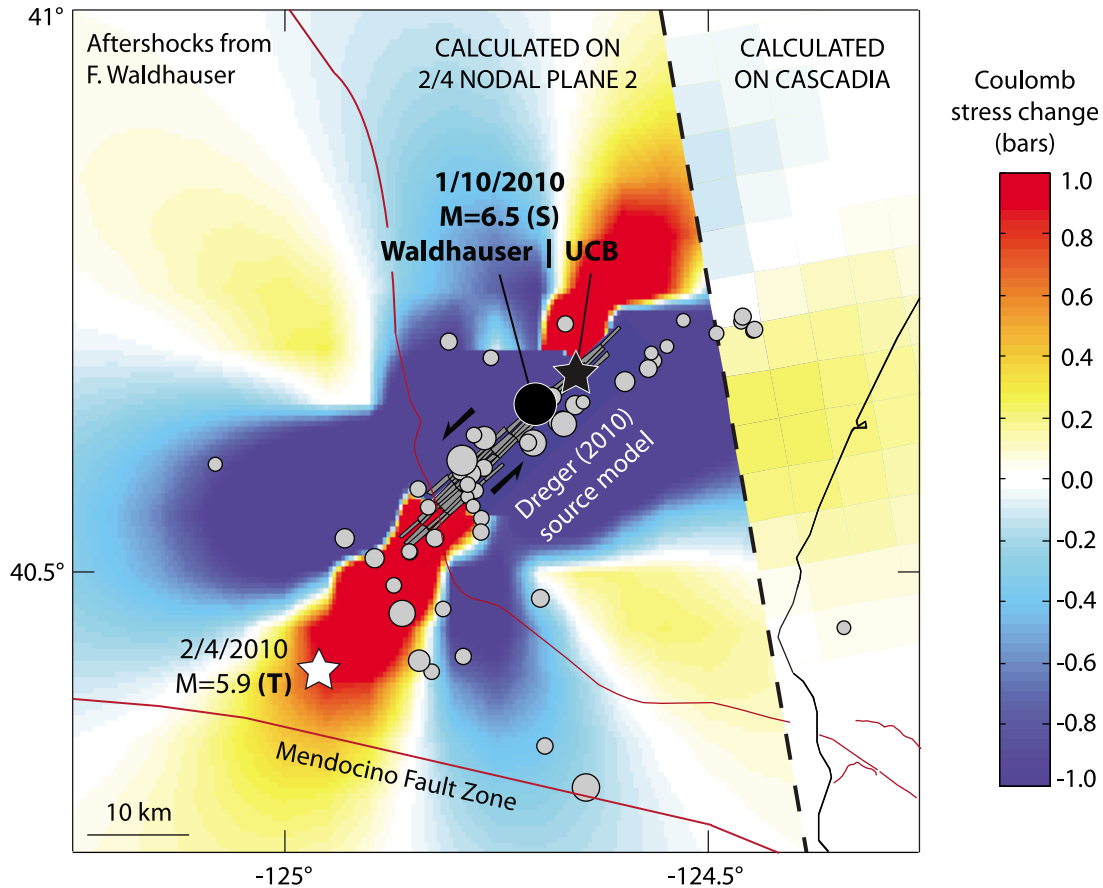


Figure 8. Coulomb stress changes imparted by the D. Dregger (unpublished report, 2010, available at http://seismo.berkeley.edu/~dregger/jan10210_ff_summary.pdf) model for the January 2010 $M=6.5$ shock (S) to nearby faults. East of the dashed line, stress changes are resolved on the Cascadia subduction zone, represented by a northward extension of the *Oppenheimer et al.* [1993] rupture plane for the 1992 $M_w=6.9$ Cape Mendocino earthquake. West of the dashed line, stress changes are resolved on the NW striking nodal plane for the February 2010 $M_w=5.9$ earthquake (T) at a depth of 23.6 km.

fault aftershock cluster. In addition, the main shock imparted a 0.2 bar Coulomb stress increase to the Cascadia subduction zone at 6–7 km depth southwest of Eureka, California.

6.9.2. Stress changes Imparted to the 4 February 2010 $M_w=5.9$ Earthquake (T)

[34] The 4 February 2010 $M_w=5.9$ earthquake (T) occurred on either a NW or SW striking fault; its aftershocks do not define a linear trend. We find that the January $M=6.5$ earthquake imparted Coulomb stress increases of 0.9 bar to the NW striking nodal plane for T and 0.6 bar to the SW striking nodal plane (Figure 8 and Table 2).

6.10. Other Cases of Large but Poorly Constrained Coulomb Stress Transfer

[35] Two other $M \geq 5.9$ earthquakes occurred very close to the rupture areas of previous earthquakes: L occurred close to K and R occurred close to D (Table 2). In these cases, possible errors in locations and rupture areas exceed the

distances between the two earthquakes, so these stress interactions, although strong, cannot be calculated reliably.

7. Location-Randomized Control Tests

[36] Given a random set of 20 independent but closely spaced $M \geq 5.9$ earthquakes, how many ≥ 0.6 bar Coulomb stress interactions would appear to occur between earthquakes less than 9 months apart? We run three control tests in which we assign the recent $M \geq 5.9$ earthquakes random epicenter locations between 40.25°N and 42.5°N latitude and between 124°W and 127°W longitude, an area in which all of the recent $M \geq 5.9$ earthquakes occurred (Figure S1). The orientations of the source models with respect to the epicenters are kept the same as in the actual 1976–2010 sequence, except that if two location-randomized source models intersect, we rotate one of the two models 180° about its epicenter. The magnitudes, rupture dimensions and

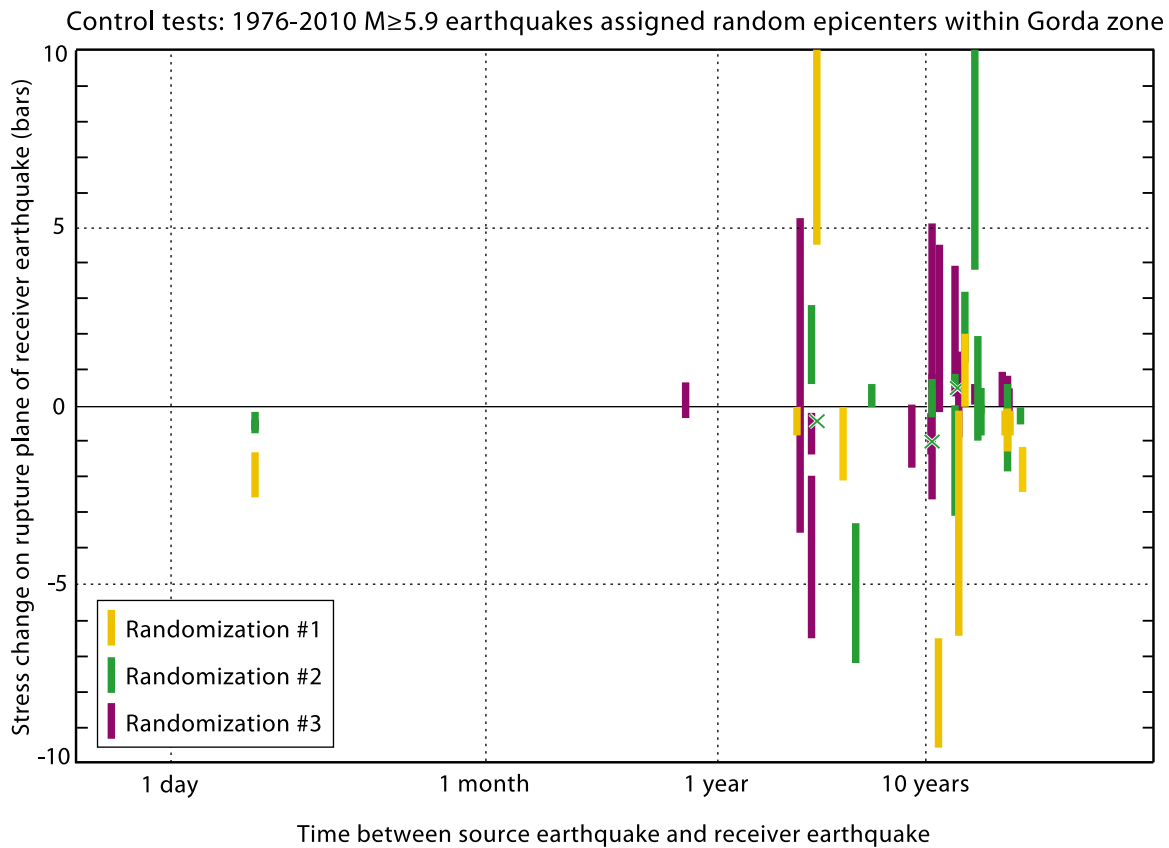


Figure 9. Coulomb stress changes of magnitude ≥ 0.5 bars between $M \geq 5.9$ earthquakes in three location-randomized control tests. The crosses and axes serve the same purposes as in Figure 3. Note the absence of cases of ≥ 0.6 bar promotion among pairs of earthquakes separated by < 1 year, compared to six cases of ≥ 0.6 bar short-term promotion in Figure 3.

orientations, and dates of the earthquakes are the same as in the actual sequence. We run this procedure three times to generate three dissimilar, essentially random distributions of the recent $M \geq 5.9$ earthquakes.

[37] Four earthquakes in set 2 and five earthquakes in set 3 are nominally promoted ≥ 0.6 bar by previous shocks, suggesting that it is possible for as many as eight $M \geq 5.9$ shocks in a set of 20 to appear to be promoted ≥ 0.6 bar by previous earthquakes (Figure 9 and Tables S1–S3). However, the control tests do not reproduce the high number of ≥ 0.6 bar positive Coulomb interactions between earthquakes < 9 months apart: only one such case is observed between

the three control tests, compared to six in the actual 1976–2010 sequence (Table 4).

8. Coulomb Stress Changes Imparted by the 1906 San Francisco Earthquake

[38] The great 1906 earthquake ruptured the San Andreas Fault to the Mendocino Triple Junction and may have imparted long-lasting stress changes to nearby faults (Figure 10). We use the *Song et al.* [2008] slip model; the northernmost 40 km of this model deviates by 5–10 km from the San Andreas Fault trace in the USGS Quaternary Fault and Fold

Table 4. Comparison of Coulomb Stress Interactions in Actual 1976–2010 Sequence and Control Tests

Set of $M \geq 5.9$ Earthquakes	Actual 1976–2010 Sequence	Control set 1	Control Set 2	Control Set 3
Number of earthquakes promoted ≥ 0.6 bar	8	1	4	5
On < 9 month timescale	(6)	-	-	(1)
Number of earthquakes inhibited ≥ 0.6 bar	1	7	5	4
On < 9 month timescale	-	(2)	(1)	-
Number of earthquakes promoted and inhibited ≥ 0.6 bar on different sections of source fault	-	-	-	3
On < 9 month timescale	-	-	-	-
Total	15	8	9	12

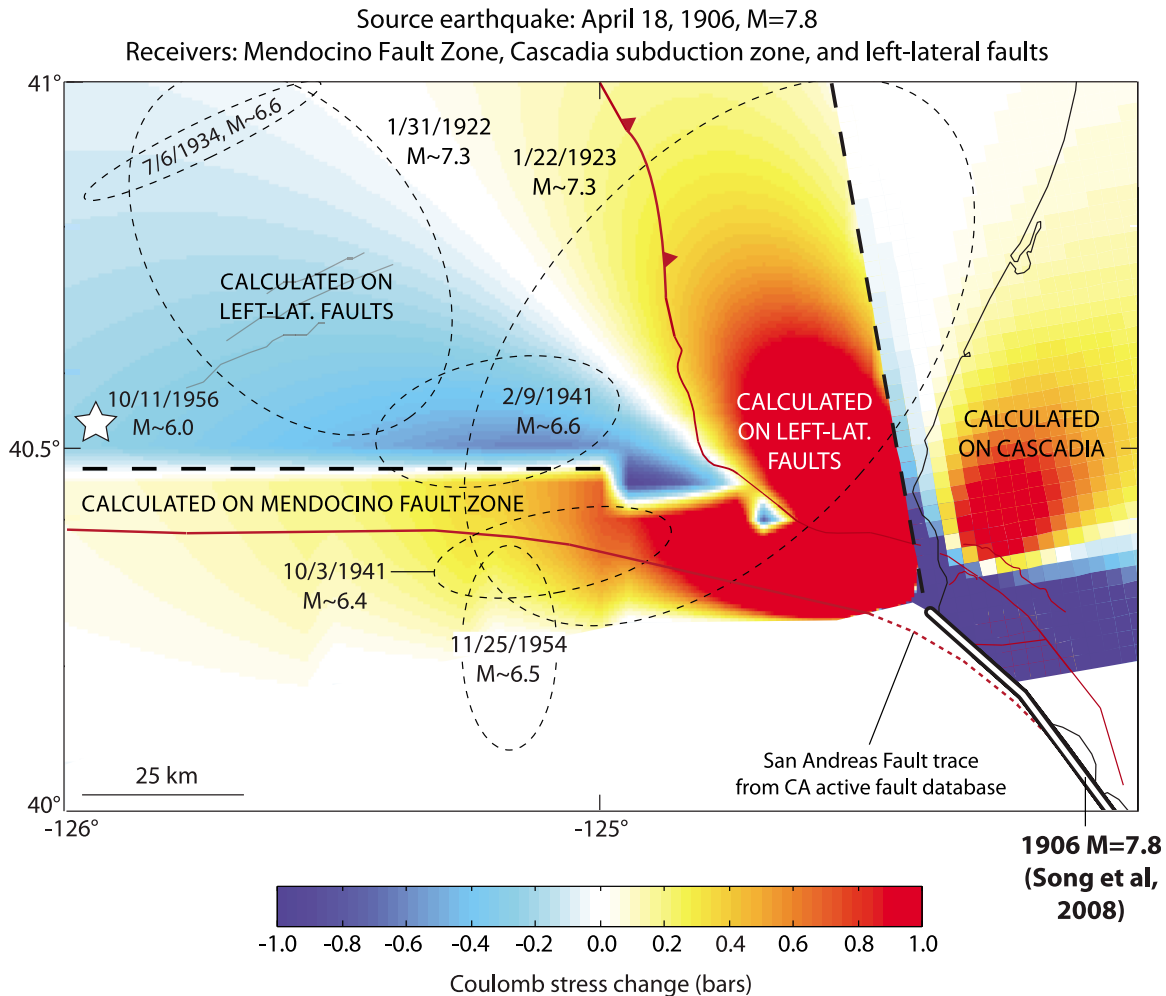


Figure 10. Coulomb stress changes imparted by the 1906 San Andreas earthquake to the Mendocino Fault Zone, the Cascadia megathrust, and northeast striking left-lateral faults within the Gorda zone. The fault matrix is the same as that used in Figure 4, except that the Cascadia subduction zone is represented by a northward and downdip extension of the *Oppenheimer et al.* [1993] rupture plane, as in Figure 8. Ellipses are 95% confidence contours for 1922–1961 $M > 6$ earthquakes from D. I. Doser (manuscript in preparation, 2010). Calculation depth is 5 km.

Database (Figure 10). We calculate that the 1906 earthquake increased stress on the Mendocino Fault Zone and both increased and decreased stress on Gorda zone left-lateral faults depending on location. These stress changes may be consistent with the locations of large offshore earthquakes in 1923, 1941 and 1954, but are inconsistent with other shocks in 1922, 1934, 1941 and 1956 (D. I. Doser, manuscript in preparation, 2010). In addition, the *Song et al.* [2008] source increases stress by >1 bar on the Cascadia megathrust north of 40.35°N latitude and decreases stress on the megathrust south of it. This is roughly consistent with the results of *Goldfinger et al.* [2008], who used the *Thatcher et al.* [1997] model for the 1906 earthquake.

9. Dynamic Triggering?

[39] In 1991, a $M_w = 6.3$ shock offshore Crescent City, California (G), was followed 21 h later by the $M_w = 6.1$ Honeydew earthquake (H) 200 km to the southeast, well outside the range of static stress interaction (Figure 1).

Dynamic interaction between these two earthquakes is possible, although H is in a direction perpendicular to the northeast/southwest rupture propagation of G. No seismicity is observed at the future site of H during the 21 h between the two earthquakes.

10. Discussion

10.1. Influence of Coulomb Stress Changes on $M \geq 5.9$ Earthquakes

[40] Control tests show that it is possible for eight $M \geq 5.9$ shocks in a random set of 20 to appear to be promoted ≥ 0.6 bar by previous earthquakes in the set, but highly unlikely for six earthquakes to appear to be promoted ≥ 0.6 bar by earthquakes < 9 months before. This indicates that the calculated Coulomb stress promotions of earthquakes J, K, L, N, Q, and T in the 1976–2010 Gorda zone sequence, if they are correct, are unlikely to be an apparent effect, and that imparted Coulomb stress changes probably influenced the timing and location of these six earthquakes. Only stress

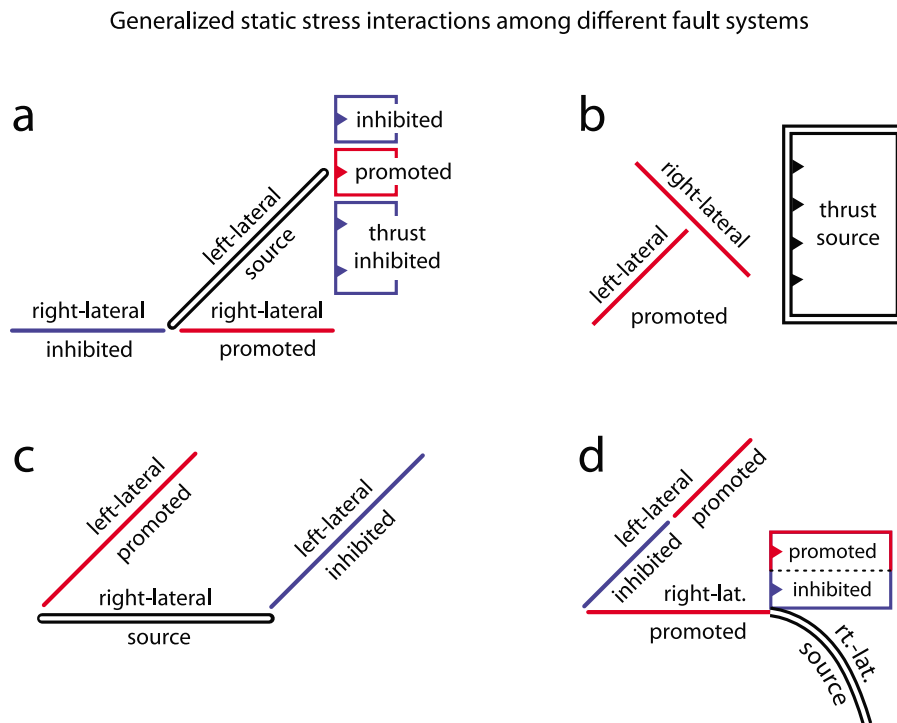


Figure 11. Generalized Coulomb stress interactions between faults of different orientations and rakes based on observations in the Gorda deformation zone.

interactions on <1 year timescales stand out from the randomized control tests, suggesting that static stress change may typically influence seismicity for periods on the order of a year in the Gorda deformation zone, consistent with the observations of *Harris et al.* [1995] in southern California. However, the absence of $M \geq 5.9$ earthquakes in the stress shadow of the 1980 $M_w = 7.3$ earthquake (B) until at least 1995 suggests that the longevity of static stress changes may increase for the largest main shocks, perhaps because they trigger viscoelastic deformation that can eventually amplify the coseismic stress changes [*Chan and Stein, 2009*].

10.2. Promotion of Aftershocks off the Source Fault

[41] Most of the 1980 $M_w = 7.3$ earthquake's elbow-shaped aftershock pattern can be correlated with Coulomb stress changes imparted to the right-lateral Mendocino Fault Zone and nearby left-lateral faults. Stress changes imparted by the January 2010 Ferndale earthquake are also somewhat consistent with a band of aftershocks perpendicular to the source. This suggests that Coulomb stress changes can trigger small earthquakes on faults nonparallel to the source, in addition to promoting large subsequent earthquakes.

10.3. Generalized Coulomb Interactions Among Different Fault Systems

[42] Observations of stress interactions between faults in this region can be applied to triple junctions and similar tectonic settings elsewhere (Figure 11). An earthquake on a northeast striking left-lateral fault increases Coulomb stress on right-lateral faults to the south but decreases stress on right-lateral faults to the southwest, and a strike-slip earthquake in a subducting slab increases stress on a localized

section of the subduction zone above it (Figure 11a). An earthquake on a north striking thrust fault increases Coulomb stress on northeast striking left-lateral faults and northwest striking right-lateral faults to the west (Figure 11b). An earthquake on an east striking right-lateral fault increases stress on left-lateral faults north of the rupture but decreases stress on left-lateral faults to the northeast (Figure 11c). A large earthquake on the northernmost San Andreas increases stress on the eastern Mendocino Fault Zone and both increases and decreases stress on the Cascadia megathrust and Gorda zone left-lateral faults depending on location (Figure 11d).

11. Conclusion

[43] We find that ≥ 0.6 bar Coulomb stress increases probably influenced the timing and location of at least 6 of 20 recent $M \geq 5.9$ earthquakes in the Gorda deformation zone. The occurrence of several other $M \geq 5.9$ earthquakes may have been indirectly influenced by the stress shadow imparted by the 1980 $M_w = 7.3$ earthquake, which may have lasted until 1995 or later. Stress changes imparted by the 1980 earthquake are also consistent with off-fault aftershocks on and around the right-lateral Mendocino Fault Zone. These findings indicate that earthquake interaction by static stress transfer can occur among faults of differing orientations, rakes and depths. Static stress changes may affect seismicity for periods on the order of 1 year in the Gorda zone, and perhaps for over a decade in the case of $M > 7.2$ earthquakes. The generalized static stress interactions derived from our observations of the 1976–2010

Gorda zone sequence may be applied to seismicity at similar tectonic settings elsewhere.

Appendix A

A1. Rupture Models

A1.1. Earthquake A: 26 November 1976, $M_w = 6.7$, off Trinidad, California

[44] The Global CMT focal mechanism and *Chaytor et al.* [2004] mapped faults suggest that this earthquake occurred on a NE striking left-lateral fault. NEIC aftershock locations are inconsistent with this orientation, but aftershock locations from the TERA Corporation [*Smith et al.*, 1982; R. C. McPherson, personal communication, 2010] are consistent with a NE striking fault plane and somewhat consistent with the NEIC main shock location. We make a tentative source model 40 km in length with the NEIC main shock location at the centroid.

A1.2. Earthquake B: 8 November 1980, $M_w = 7.3$, off Trinidad, California

[45] Our model for this earthquake is based primarily on the aftershock pattern shown in the plot of 1980–1986 northern California seismicity of *Eaton* [1987] and *Hill et al.* [1990], with relocations by J.P. Eaton using phase data from the TERA Corporation and NCSN (Figure 2, earthquakes A and B). The aftershock distribution contains four distinct clusters, hereafter referred to by the numbering system used in Figures 2 (earthquake A) and 4. Clusters 1 and 2 define a N50°E trend consistent with the Global CMT focal mechanism and are inferred to be on the rupture. Cluster 1, which trends northeast from 41°N, 124.9°W and includes the main shock hypocenter, is east of the surface trace of the Cascadia subduction zone, indicating that the northeastern section of the rupture occurred in the subducting Gorda slab. Cluster 2 is southwest of cluster 1 and continues the N50°E trend; however, *Chaytor et al.* [2004] mapped faults strike ~65° nearby, suggesting that the southwest section of the rupture may have bent toward a more easterly strike. Clusters 3 and 4, inferred to be off the rupture because of their orientations and locations, are described in section 6. Assuming a bilateral rupture after *Lay et al.* [1982], we choose a 100 km long source model extending 77 km southwest and 23 km northeast from the NCSN epicenter. The model strikes 51° in the northeastern 70 km and plunges under the Cascadia subduction zone in the northeasternmost 50 km. The megathrust is assumed to strike 350° and dip 9°, so a vertical fault striking 51° within the downgoing slab would plunge 7.5° along strike; the model simulates this plunge by “stepping down” 1 km for every 7.7 km along strike. The model strikes 65° in the southwest 30 km, following *Chaytor et al.* [2004] mapped faults.

A1.3. Earthquake C: 24 August 1983, $M_w = 6.1$, off Petrolia, California

[46] The main NCSN aftershock cluster is 10–25 km offshore at 20–30 km depth, but the NCSN main shock location lies 50 km offshore at 12 km depth (Figure 2, earthquake C). The NEIC main shock location, which uses data from 217 stations to the NCSN location’s 42, is 30 km offshore at 30 km depth. Our model extends updip and eastward from the NEIC hypocenter, consistent with NCSN

aftershocks. Because of potential errors in NCSN aftershock locations, stress interactions using this model are poorly constrained.

A1.4. Earthquake D: 10 September 1984, $M_w = 6.6$, Mendocino Fault Zone

[47] The NEIC epicenter is on the Mendocino Fault Zone, consistent with the Global CMT focal mechanism, but NEIC aftershock locations are 10–20 km south of the fault zone, so we do not make a source model for this earthquake (Figure 2, earthquake D).

A1.5. Earthquake E: 31 July 1987, $M_w = 6.0$, off Petrolia, California

[48] The NCSN hypocenter is on the northeast part of the aftershock pattern in the northern California double-difference catalog [*Waldhauser and Schaff*, 2008] (Figure 2, earthquake E). The source model which best fits the aftershock pattern has the hypocenter located 80% of the way to the northeast corner of the rupture and 80% of the way to the top of the rupture.

A1.6. Earthquake F: 13 July 1991, $M_w = 6.8$, off Brookings, Oregon

[49] The northeasternmost NEIC aftershocks suggest a strike of 225°, consistent with the Global CMT focal mechanism, but aftershocks southwest of the epicenter trend 195°; local *Chaytor et al.* [2004] faults feature both orientations (Figure 2, earthquake F). We make two alternate source models: (1) a 40 km long straight rupture striking 225° with the NEIC epicenter at the centroid and (2) a 55 km long rupture whose strike changes from 225° to 195° 12 km southwest of the epicenter.

A1.7. Earthquake G: 16 August 1991, $M_w = 6.3$, off Crescent City, California

[50] The NEIC main shock location is more reliable than the NCSN location at this distance (>100 km) offshore, but NEIC aftershock locations are inconsistent with the NEIC epicenter, so we do not make a source model for this earthquake (Figure 2, earthquake G).

A1.8. Earthquake H: 17 August 1991 (1929 UTC), $M_w = 6.1$, Honeydew, California

[51] The aftershock pattern in the double-difference catalog [*Waldhauser and Schaff*, 2008] trends northwest and dips northeast, consistent with the Global CMT focal mechanism (nodal plane 1) (Figure 2, earthquake H). *McPherson and Dengler* [1992] suggest a southwest or west dipping rupture plane based on local fault orientations and observed effects at the surface. This orientation is compatible with the second nodal plane in the Global CMT focal mechanism, but it is not consistent with the aftershock pattern, and so we choose a northeast dipping model that uses the double-difference main shock location as the lower eastern corner of the rupture plane. Aftershock locations suggest that the rupture propagated updip and west, a similar rupture direction to the 1992 Cape Mendocino earthquake [*Oppenheimer et al.*, 1993].

A1.9. Earthquake I: 17 August 1991 (2217 UTC), $M_w = 7.1$, off Crescent City, California

[52] The NEIC main shock location is more reliable than the NCSN location at this distance (>100 km) offshore, but NEIC aftershock locations are inconsistent with the NEIC epicenter, so we do not make a source model for this earthquake (Figure 2, earthquake I).

A1.10. Earthquake J: 25 April 1992, $M_w = 6.9$, Cape Mendocino, California

[53] We use the *Oppenheimer et al.* [1993] slip model and taper the slip at the edges (Figure 2, earthquake J).

A1.11. Earthquake K: 26 April 1992 (0741 UTC), $M_w = 6.5$, off Cape Mendocino, California

[54] The hypocenter in the northern California double-difference catalog [*Waldhauser and Schaff*, 2008] is at the northwestern end of the aftershock distribution (Figure 2, earthquakes K and L). Based on the double-difference aftershock pattern, Figure 3b of *Oppenheimer et al.* [1993], and the apparent stress of 40 bars calculated by *Choy and McGarr* [2002], we choose a rupture 12.5 km long and 6.25 km wide extending southeast from the epicenter. Few aftershocks were recorded at the depth of this earthquake in the 3.5 h period between this shock and L, and they do not define a linear pattern, so this model is poorly constrained.

A1.12. Earthquake L: 26 April 1992 (1118 UTC), $M_w = 6.6$, off Cape Mendocino, California

[55] The apparent stress of 164 bars calculated by *Choy and McGarr* [2002] suggests a small rupture area with a high average slip (Figure 2, earthquakes K and L). Based on aftershock locations and Figure 3b of *Oppenheimer et al.* [1993], we choose a rupture 10 km wide and 5 km long extending southeast and updip from the NCSN hypocenter. A rupture plane is not visible in the cluster of aftershocks of this shock and K, so this model is poorly constrained.

A1.13. Earthquake M: 1 September 1994, $M_w = 7.0$, Mendocino Fault Zone

[56] The apparent stress of 165 bars calculated by *Choy and McGarr* [2002] suggests a small rupture area with a high average slip (Figure 2, earthquake M). The NEIC epicenter is at the center of the NEIC aftershock distribution, suggesting a bilateral rupture, while *Dengler et al.* [1995] infer that the rupture propagated unilaterally to the east. We make a model for each scenario. Each source is 15 km long and 7.5 km wide, uses the Global CMT focal mechanism and scalar moment, and has a calculated average slip of 10.7 m.

A1.14. Earthquake N: 19 February 1995, $M_w = 6.6$, Southern Gorda Zone

[57] NEIC aftershock locations are roughly consistent with the NEIC main shock location, but they do not define a linear pattern which would indicate a rupture plane (Figure 2, earthquakes N and O). We make a tentative source model which uses the NEIC main shock location as the centroid.

A1.15. Earthquake O: 16 March 2000, $M_w = 5.9$, Mendocino Fault Zone

[58] NEIC aftershocks are sparse but roughly consistent with the NEIC main shock location, so we make a tentative source model with the NEIC location at the centroid (Figure 2, earthquakes N and O).

A1.16. Earthquake P: 15 June 2005, $M_w = 7.2$, off Eureka, California

[59] We use the G. Shao and C. Ji (2005) slip model, excluding the southwest 12 km, northeast 18 km, and bottom 15 km of their 102 km \times 35 km model because of the low slip values in those sections (Figure 2, earthquakes P, Q, and R).

A1.17. Earthquake Q: 17 June 2005, $M_w = 6.6$, Southwest Gorda Zone

[60] The Global CMT focal mechanism is consistent with the orientation of *Chaytor et al.* [2004] mapped faults near the epicenter, but NEIC aftershock locations are sparse (Figure 2, earthquakes P, Q, and R). We make a tentative source model with the NEIC location at the centroid.

A1.18. Earthquake R: 28 November 2008, $M_w = 5.9$, Mendocino Fault Zone

[61] NEIC aftershocks are sparse but roughly consistent with the NEIC main shock location, so we make a tentative source model with the NEIC location at the centroid (Figure 2, earthquakes P, Q, and R).

A1.19. Earthquake S: 10 January 2010, $M = 6.5$, off Ferndale, California

[62] We use the updated D. Dreger (unpublished report, 2010, available at http://seismo.berkeley.edu/~dreger/jan102010_ff_summary.pdf) finite fault model (Figure 2, earthquakes S and T).

A1.20. Earthquake T: 4 February 2010, $M_w = 5.9$, off Cape Mendocino, California

[63] As this is the most recent $M \geq 5.9$ earthquake, we do not make a source model for this earthquake, but we calculate stress changes imparted by other earthquakes at its epicenter (Figure 2, earthquakes S and T).

A2. Large Historical Earthquakes

[64] Locations and focal mechanisms are too poorly constrained to support source models for earthquakes in the Gorda zone before 1976, but we consider two very large pre-1976 shocks for which slip models have been built based on coseismic deformation.

A2.1. The 26 January 1700, $M \sim 9$, Cascadia Subduction Zone

[65] The most detailed model for the 1700 Cascadia earthquake [*Pollitz et al.*, 2008] is made up of 115 km long rectangular patches with slip vectors calculated from fitting of a postseismic viscoelastic model. Stress changes imparted by this model are unreliable close to the source because they are controlled by the straight edges of the patches. Additionally, the margin of uncertainty in the 1700 slip distribution exceeds the size of the Gorda deformation zone itself. For these reasons, we cannot reliably calculate the stress change imparted to Gorda zone faults by the 1700 earthquake.

A2.2. The 18 April 1906, $M = 7.8$, San Andreas Fault

[66] To calculate the Coulomb stress changes imparted by the 1906 San Andreas earthquake to the Gorda deformation zone, we use the *Song et al.* [2008] variable slip model, which is determined from a joint geodetic and seismic inversion. The northernmost 40 km of this model deviates by 5–10 km from the San Andreas Fault trace in the USGS Quaternary Fault and Fold Database (Figure 2, earthquake Z).

[67] **Acknowledgments.** We thank David Oppenheimer, Patricia McCrory, and Ruth Harris for reviews; Volkan Sevilgen and Shinji Toda for technical assistance; Chris Goldfinger and Jason Chaytor for active fault data; Felix Waldhauser and David Schaff for the double-difference catalog; and Robert McPherson, Charles Sammis, and Lori Dengler for input.

References

- Cande, S. C., and D. V. Kent (1995), Revised calibration of the geomagnetic polarity timescale for the Late Cretaceous and Early Cenozoic, *J. Geophys. Res.*, *100*(B4), 6093–6095, doi:10.1029/94JB03098.
- Chan, C. H., and R. S. Stein (2009), Stress evolution following the 1999 Chi-Chi, Taiwan, earthquake: Consequences for afterslip, relaxation, aftershocks, and departures from Omori decay, *Geophys. J. Int.*, *177*, 179–192, doi:10.1111/j.1365-246X.2008.04069.x.
- Chaytor, J. D., C. Goldfinger, R. P. Dziak, and C. G. Fox (2004), Active deformation of the Gorda plate: Constraining deformation models with new geophysical data, *Geology*, *32*, 353–356, doi:10.1130/G20178.2.
- Choy, G. L., and A. McGarr (2002), Strike-slip earthquakes in the oceanic lithosphere: Observations of exceptionally high apparent stress, *Geophys. J. Int.*, *150*, 506–523, doi:10.1046/j.1365-246X.2002.01720.x.
- Dengler, L., K. Moley, R. McPherson, M. Pasyanos, J. W. Dewey, and M. Murray (1995), The September 1, 1994 Mendocino Fault earthquake, *Calif. Geol.*, *48*, 43–53.
- Eaton, J. P. (1987), Dense microearthquake network study of northern California earthquakes, in *Observatory Seismology*, pp. 200–225, Univ. of Calif. Press, Berkeley.
- Goldfinger, C., et al. (2008), Late Holocene rupture of the San Andreas Fault and possible stress linkage to the Cascadia Subduction Zone, *Bull. Seismol. Soc. Am.*, *98*, 861–889, doi:10.1785/0120060411.
- Harris, R. A., R. W. Simpson, and P. A. Reasenberg (1995), Influence of static stress changes on earthquake locations in southern California, *Nature*, *375*, 221–224, doi:10.1038/375221a0.
- Henstock, T. J., and A. Levander (2003), Structure and seismotectonics of the Mendocino Triple Junction, California, *J. Geophys. Res.*, *108*(B5), 2260, doi:10.1029/2001JB000902.
- Hill, D. P., J. P. Eaton, and L. M. Jones (1990), Seismicity, 1980–1986, in *The San Andreas Fault System, California*, edited by R. E. Wallace, *U.S. Geol. Surv. Prof. Pap.*, *1515*, 115–151.
- Jachens, R., and A. Griscom (1983), Three-dimensional geometry of the Gorda Plate beneath northern California, *J. Geophys. Res.*, *88*(B11), 9375–9392, doi:10.1029/JB088iB11p09375.
- King, G. C. P., R. S. Stein, and J. Lin (1994), Static stress changes and the triggering of earthquakes, *Bull. Seismol. Soc. Am.*, *84*, 935–953.
- Lay, T., J. W. Given, and H. Kanamori (1982), Long-period mechanism of the November 8, 1980 Eureka, California earthquake, *Bull. Seismol. Soc. Am.*, *72*, 439–456.
- McCrory, P. A., J. L. Blair, D. H. Oppenheimer, and S. R. Walter (2004), Depth to the Juan De Fuca slab beneath the Cascadia Subduction Margin—A 3-D model for sorting earthquakes, *Data Series DS-91*, version 1.1, U.S. Geol. Surv., Menlo Park, Calif.
- McPherson, R. C., and L. A. Dengler (1992), The Honeydew earthquake, *Calif. Geol.*, *45*, 31–39.
- Oppenheimer, D. H., et al. (1993), The Cape Mendocino, California, earthquakes of April 1992: Subduction at the triple junction, *Science*, *261*, 433–438, doi:10.1126/science.261.5120.433.
- Pollitz, F. F., P. McCrory, J. Svarc, and J. Murray (2008), Dislocation models of interseismic deformation in the western United States, *J. Geophys. Res.*, *113*, B04413, doi:10.1029/2007JB005174.
- Smith, S. W., R. C. McPherson, M. Niazi, and N. Severy (1982), The November 1980 Trinidad offshore earthquake and aftershocks, technical report, Pac. Gas and Electr., San Francisco, Calif.
- Smith, S. W., J. S. Knapp, and R. C. McPherson (1993), Seismicity of the Gorda Plate, structure of the continental margin, and an eastward jump of the Mendocino Triple Junction, *J. Geophys. Res.*, *98*, 8153–8171, doi:10.1029/93JB00026.
- Song, S. G., G. C. Beroza, and P. Segall (2008), A unified source model for the 1906 San Francisco earthquake, *Bull. Seismol. Soc. Am.*, *98*, 823–831, doi:10.1785/0120060402.
- Stein, R. S., A. A. Barka, and J. H. Dieterich (1997), Progressive failure on the North Anatolian fault since 1939 by earthquake stress triggering, *Geophys. J. Int.*, *128*, 594–604, doi:10.1111/j.1365-246X.1997.tb05321.x.
- Thatcher, W., G. Marshall, and M. Lisowski (1997), Resolution of fault slip along the 470-km-long rupture of the great 1906 San Francisco earthquake and its implications, *J. Geophys. Res.*, *102*, 5353–5367, doi:10.1029/96JB03486.
- Waldhauser, F., and D. P. Schaff (2008), Large-scale relocation of two decades of Northern California seismicity using cross-correlation and double-difference methods, *J. Geophys. Res.*, *113*, B08311, doi:10.1029/2007JB005479.
- Wells, D. J., and K. J. Coppersmith (1994), New empirical relationships among magnitude, rupture length, rupture width, rupture area, and surface displacement, *Bull. Seismol. Soc. Am.*, *84*, 974–1002.
- Wilson, D. S. (1986), A kinematic model for the Gorda Deformation Zone as a diffuse southern boundary of the Juan de Fuca Plate, *J. Geophys. Res.*, *91*, 10,259–10,269, doi:10.1029/JB091iB10p10259.
- Wilson, D. S. (1989), Deformation of the so-called Gorda Plate, *J. Geophys. Res.*, *94*, 3065–3075, doi:10.1029/JB094iB03p03065.

J. C. Rollins, Department of Earth Sciences, University of Southern California, 3651 Trousdale Pkwy., Los Angeles, CA 90089-0740, USA. (chrisrol@usc.edu)

R. S. Stein, U.S. Geological Survey, 345 Middlefield Rd., MS 977, Menlo Park, CA 94025, USA. (rstein@usgs.gov)